Genetic-Algorithm Discovery of a Direct-Gap and Optically Allowed Superstructure from Indirect-Gap Si and Ge Semiconductors

Mayeul d'Avezac and Jun-Wei Luo
National Renewable Energy Laboratory, Golden, Colorado 80401, USA

Thomas Chanier
Department of Physics and Astronomy, University of Iowa, 203 VAN, Iowa City, Iowa 52242, USA

Alex Zunger
University of Colorado, Boulder, Colorado 80401, USA
(Received 9 July 2011; published 12 January 2012)

Combining two indirect-gap materials—with different electronic and optical gaps—to create a direct gap material represents an ongoing theoretical challenge with potentially rewarding practical implications, such as optoelectronics integration on a single wafer. We provide an unexpected solution to this classic problem, by spatially melding two indirect-gap materials (Si and Ge) into one strongly dipole-allowed direct-gap material. We leverage a combination of genetic algorithms with a pseudopotential Hamiltonian to search through the astronomic number of variants of $Si_n/Ge_m/\ldots/Si_p/Ge_q$ superstructures grown on (001) $Si_{1-x}Ge_x$. The search reveals a robust configurational motif—$SiGe_2Si_2Ge_2SiGe_n$ on (001) Si_xGe_{1-x} substrate ($x \leq 0.4$) presenting a *direct* and *dipole-allowed* gap resulting from an enhanced Γ-X coupling at the band edges.

DOI: 10.1103/PhysRevLett.108.027401 PACS numbers: 78.67.Bf, 73.63.Bd, 78.40.Fy

The fact that silicon is the paradigm semiconductor—readily dopable by either electrons or holes and protected from environmental scatterers by a native oxide passivation layer—is unfortunately not matched by the additional virtue of being able to strongly emit and absorb light. Nevertheless, one of the outstanding projects of the semiconductor industry is the integration of optical and electronic functions on single-crystal silicon wafers [1,2]. We provide a new and unexpected solution to a classic problem, showing how two indirect-gap materials (Si and Ge) can be spatially melded together into one strongly dipole-allowed direct-gap material.

There are three main routes to integrating optical functions—and specifically light emission—onto a silicon wafer. The "device" route relies on a strong external magnetic field to instigate electron-hole recombination despite silicon's indirect gap through either field emission—e.g., tunneling between electron and hole bands—or electron avalanches [2]. The second route relies on introducing local recombination centers into the material, thus bypassing altogether the constraints imposed on the optical spectra by silicon's band structure. In practice, this has been achieved through rare-earth doping, such as erbium [3], or by engineering dislocations into the silicon wafer [1].

The third route prefers to manipulate the band structure of silicon directly to create a material with optically active band edges. For example, in an indirect material where the gap at γ and the indirect gap are fairly close in energy, such as germanium (and unlike silicon), uniaxial tensile strain alone is sufficient to lower the conduction band at γ below the CBM [4]. Another example is nanostructuring where one attempts to relax the constraints imposed by translational invariance and conservation of momentum. Indeed, nanostructuring is the basis of large body of literature which purports to create direct-gap silicon in nanowires, quantum dots, or exotic nanostructures such as nanonets [5]. Unfortunately, and as we will see later, relaxing translational symmetries is simply not sufficient to create an *optically* active structure, as evidenced years later in the case of nanonets [6]. Finally, alloying with other group IV atomic species, such as tin and germanium [7], introduces extra degrees of freedom to modify the band structure.

The combination of nanostructuring, alloying, and strain did yield a superlattice, Si_6Ge_4, which, when grown under (001) epitaxial strain, displays a small but nonzero absorption at the band-edges [8,9]. However, despite this relative success—the coupling between CBM and VBM is too small for actual applications—further studies were not carried out beyond single-repeat-period motifs $[Si_nGe_m]_\infty$. The difficulty resides in identifying the one genomic sequence of Si and Ge layers with the right code for strong transition across the electronic band-gap from amongst all possible superlattices $[Si_{n_0}Ge_{p_0}/Si_{n_1}Ge_{p_1}/\ldots/Si_{n_N}Ge_{p_N}]_\infty$, including substrate orientation and strain. This problem could not have been solved previously [8–10] because the tools for exploring such large spaces ($\backsim 2^N$ for N layers on a given substrate) did not exist.

In this work, we use computer-assisted search methods to explore the $Si_{n_0}/Ge_{m_0}/\ldots/Si_{n_N}/Ge_{m_N}$ motifs with the

explicit goal of finding a direct-gap and optically active material. Using a combination of genetic algorithms [11] and band-structure calculation [12], we identify a motif with a 50-fold increase of the dipole matrix element over the previous record set by Si_6Ge_4. This motif is a dipole-allowed direct-gap material with a light efficiency (as defined by the momentum matrix) of 10% compared to the *direct* transition at Γ of bulk Si, yet it should retain electronic transport properties similar to Si, as evidenced by the calculated effective masses. We show that the conduction band minimum (CBM) is mostly located on Si, and thus that the epitaxial structure is indeed silicon made direct. The discovery of a genetically engineered wave vector-direct *and* strong dipole-allowed layered structure made of common indirect-gap components represents a step forward in combining opto-electronic components on a single Si wafer [13,14]. It opens the way for similar searches in other difficult cases. Experimental synthesis of this magic motif, say through molecular beam epitaxy, is called for.

Method.—Exploring the large and complex space of all possible Si/Ge superlattices requires an efficient search method. We turn to a bit string genetic algorithm [12] (GA) which emulates Darwinian evolution *in silica* by constructing and refining a population of superlattices according to chance and their relative fitness to our purpose, namely, their propensity for light-emission at the band-edges. New superlattice candidates (offspring) are created from the previous population by swapping random sets of layers in the superlattice between two parents (crossover), and by flipping random Ge layers into Si layers and vice-versa in a single parent (mutation). At each generation, the worst individuals in the previous population are replaced by the offspring, thus guiding the population as a whole towards the global optimum through survival of the fittest. To judge fitness, i.e., the strength of the optical transition, we compute the dipole matrix element between the VBM and CBM at Γ of each superlattice candidate. This quantity is directly proportional to the strength of the optical transition. It is null in the case of "false positives" where the gap is wave vector direct as a result of folding yet optically inactive. The dipole matrix elements are computed using the momentum approximation [15] with a an atomistic pseudopotential Hamiltonian [16], fitted (to remove DFT errors) to interband transition energies, effective masses, deformation potentials, band-offsets, as well as the bulk single-particle wave functions described by density functional theory within the local density approximation. This screened potential, in conjunction with a plane-wave basis set and folded-spectrum diagonalization, allows us to predict accurate dipole matrix elements for fairly large systems (≥ 80 atoms) with sufficient efficiency that we can perform literally hundreds of thousands of calculations during the course of the GA search. The virtual-substrate-bound superlattices are strain relaxed using a previously parameterized valence force field method [17]. GA searches are performed for (001) $Si_{1-x}Ge_x$ virtual substrates with different lattice constants, and for superlattices with either 20 or 40 monolayers (in 001 direction). To ensure convergence, at least three independent GA searches are performed for each substrate and periodicity.

The magic sequence and its properties.—The GA search reveals a number of periodic sequences with high dipole matrix element. All, however, are variations of a *magic sequence* composed of an active motif $SiGe_2Si_2Ge_2Si$ followed by a Germanium buffer layer of $n = 12$–32 monolayers. In the following, we report all results for $n = 12$, as a matter of simplicity. The magic sequence satisfies (i) wave vector directness and (ii) the dipole matrix element between the VBM and the CBM is nonzero, as shown in Fig. 1. The first condition is satisfied when the structure is grown on substrates $Si_{1-x}Ge_x$, for Germanium rich substrates with $x \geq 0.4$, as illustrated by the band structure in Fig. 1. For more silicon-rich substrates, the conduction band at X in the epitaxial plane slips below Γ. The exact lattice parameter of the freestanding magic sequence will be depend of course on the size of the Ge buffer. However, for a buffer of 12 monolayers, as in Fig. 1, the equilibrium lattice parameter is equivalent to $Si_{1-x}Ge_x$, with $x = 0.2$. The second condition is evidenced by the absorption spectra in the top panel of Fig. 2. It also contains the direct absorption spectra for the current experimentally-studied state-of-the-art superlattice [18,19], Si_6Ge_4. Both include a 20 meV Gaussian broadening. We find a $\sim$50 fold increase of the latter over the former. Unlike Si_6Ge_4, this puts the magic sequence well within the range of feasibility for practical applications. It should be noted, however, that the absorption is heavily polarized, and the polarization depends strongly on the lattice constant of the underlying virtual substrate, as evidenced by the components parallel and perpendicular to

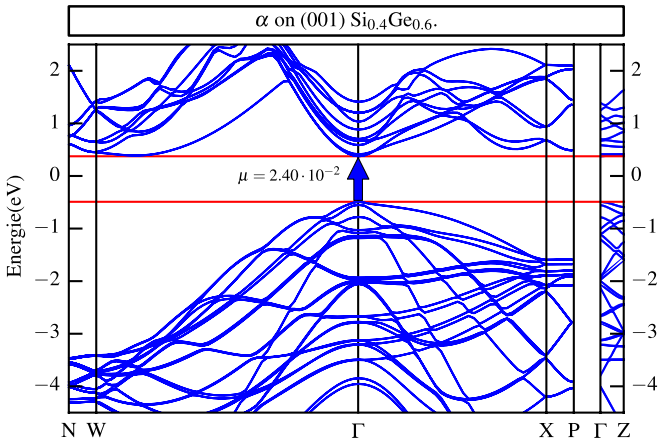

FIG. 1 (color online). Band structures of the $\alpha_{n=12}$ magic sequence grown on $Si_{0.4}Ge_{0.6}$. It is wave vector direct at $\bar{\bar{\Gamma}}$ and presents a nonzero dipole moment between the band edges. Thus it is an optically active direct-gap silicon material.

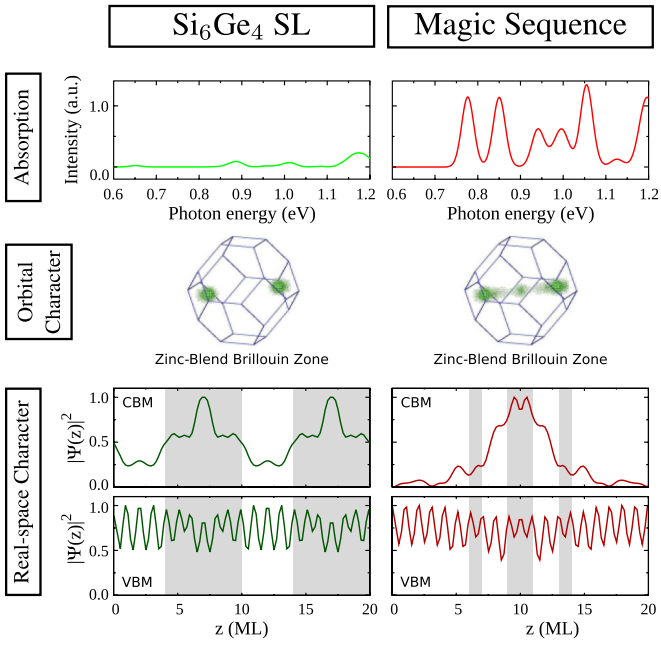

FIG. 2 (color online). Comparison of between Si_6Ge_4 superlattice [18,19] and the magic sequence discovered in this Letter (with a Ge buffer of 12 monolayers and grown on $Si_{0.4}Ge_{0.6}$). The top panel shows the direct absorption spectra (computed with a 20 meV gaussian broadening). The middle panel represents the reciprocal space orbital character of the CBM, e.g., the components of the CBM in the zinc blende Brillouin zone. The bottom most panel shows the location in real-space of the CBM and the VBM along the growth direction, with silicon layers in gray and Germanium regions in white. The CBM of both superlattices are mostly located on Si, and both contain some $\vec{\Gamma}$ character necessary for optical coupling with the VBM. However, the absorption spectra of the magic sequence is by far the largest.

the growth direction of the dipole matrix element reported in Table I. Indeed, whereas the overall magnitude of the dipole element is fairly constant for any $Si_{1-x}Ge_x$ substrate, for any concentration x, the component along the growth direction goes from being the largest on $Si_{0.6}Ge_{0.4}$ to almost extinct on the Germanium substrate. Finally, we find the electronic transport of the magic sequence will not be ill affected by the superlattice construction, since its effective masses are quite squarely between those of silicon and Germanium (see Table II).

Mechanism of the interband coupling leading to a dipole-allowed transition.—To understand how the magic sequence becomes direct and optically-active, we analyze in the middle panel of Fig. 2 the *orbital character* of the band-edges Fourier space. The orbital character, also called majority representation [20], plots the origin of the superlattice's CBM in the unfolded Brillouin zone of the zinc blende. In other words it tells us which states from the bulk-components hybridize through folding at $\bar{\Gamma}$ in the superlattice Brillouin zone. We find that in both the magic sequence and in Si_6Ge_4 the CBM at $\bar{\Gamma}$ are constructed from X and Γ states, with however a much larger contribution in the case of the latter. This result is in line with the much larger absorption from the magic sequence. The lower two panels of Fig. 2 plot the wave function density of the CBM and VBM averaged over the epitaxial plane. In both materials, the VBM is delocalize over the whole superlattice, whereas the CBM is principally located over the Si-rich region. However, in the magic sequence, this region is fairly small (two monolayers). The CBM wave function is mostly contained within the active motif itself.

Sensitivity of the results to deviation from the optimal structure.—In practice, the accuracy of the growth method could result slight variations from the optimal structure predicted in this Letter. How much would this affect the optical transition across the electronic gap? We examine the effect of changing both the virtual substrate and mutations in the magic sequence upon the optically active direct gap. In the following, α_n is the magic sequence with a Ge buffer of n monolayers, while β is the sequence $SiGe_2Si_2Ge_2SiGe_2SiGe_9$ and γ the sequence $SiGe_2SiGe_2Si_2Ge_2SiGe_2SiGe_6$. Figure 3(a) shows the "degree of directness" (left vertical axis—solid lines)—the difference between the folded $\bar{\Gamma}_c$ and the CBM of Si, $\mathbf{\Delta}_{x,y}$—and the dipole matrix element between the valence and conduction band at $\bar{\Gamma}$ (right vertical axis—dashed lines) as a function of the choice of substrate in-plane lattice parameter. Note that the dipole matrix element is between states *at* $\bar{\Gamma}$ rather than between the VBM and the CBM which may be off-$\bar{\Gamma}$. As a result, it is nonzero even in

TABLE I. Dipole matrix elements between the conduction band minimum and the valence band maximum of candidate superlattices on (001) Ge and (001) $Si_{0.4}Ge_{0.6}$ substrates, compared to the dipole moments of $\Gamma_{8v} - \Gamma_{6c}$ transition in bulk Ge. We report the dipole matrix elements $p_\parallel$ parallel to the substrate growth direction (001) and perpendicular $p_\perp$ to (001) between valence and conduction band in atomic units.

SL	Substrate	$\lvert\langle v\rvert p_\parallel \lvert c\rangle\rvert^2$	$\lvert\langle v\rvert p_\perp \lvert c\rangle\rvert^2$	$\lvert\langle v\rvert p \lvert c\rangle\rvert^2$
Ge	Ge	1.28×10^{-7}	0.185	0.37
Si_6Ge_4	Ge	5.05×10^{-4}	2.72×10^{-5}	5.59×10^{-4}
	$Si_{0.4}Ge_{0.6}$	5.21×10^{-4}	1.21×10^{-4}	7.64×10^{-4}
Magic sequence	Ge	2.46×10^{-2}	3.42×10^{-3}	3.15×10^{-2}
	$Si_{0.4}Ge_{0.6}$	1.81×10^{-7}	1.35×10^{-2}	2.71×10^{-2}

TABLE II. Effective masses of Si, Ge, the magic sequence discovered in this work, and Si_6Ge_4 at $\vec{\bar{\Gamma}}$ in the [001] direction (e.g., in the epitaxial plane) in units of m_e, the mass of the free electron at rest. All five materials are grown on the same substrate, (100) $Si_{0.4}Ge_{0.6}$ *and* within the same supercell.

Material	Electron	Heavy-hole	Light-hole
Si	$0.21m_e$	$0.27m_e$	$0.23m_e$
Ge	$0.11m_e$	$0.11m_e$	$0.09m_e$
α_{12}	$0.16m_e$	$0.16m_e$	$0.13m_e$
Si_6Ge_4	$0.18m_e$	$0.26m_e$	$0.18m_e$

the case of indirect gaps in reciprocal space. For reference, the top abscissa also gives the strain with respect to free-standing the magic sequence α_{12}, i.e., grown in bulk rather than on a substrate. α_{12}, with a content of 20% Si in the *film*, becomes direct when deposited on a substrate with more than 40% Ge content. This is a consequence of the variation in deformation potential at $\bar{\Gamma}$ and $\bar{\delta}$. The total dipole matrix element increases slowly with strain. For both quantities, the behavior of α_{12} and its variants, α_{14}, β, and γ are strikingly similar, indicating the pattern is robust with respect to mutations. Unsurprisingly, Si_6Ge_4 becomes direct much sooner, for substrates with more than 30% Ge, since its content in Si is greater. Note however that in Table I the polarization for α_{12}, β, and γ changes drastically from a $Si_{0.4}Ge_{0.6}$ substrate to the Ge substrate. It can be difficult experimentally to create perfect pure layers of Si or Ge. In practice, atoms may diffuse across layer interface in what is known as interface mixing. We model this effect in Fig. 3(b) by mapping Si to $Si_{1-x}Ge_x$ and Ge to Si_xGe_{1-x} (abscissa) over the magic pattern and its edge, defined as two monolayers thick. For $x = 0$, perfect Si and Ge monolayers are retained, whereas for $x = 0.5$ the pattern is lost completely—the distinction between Si rich and Ge rich has disappeared—and is replaced by random alloy of $Si_{0.5}Ge_{0.5}$ over a buffer of pure Ge. We plot in Fig. 3(b) the total dipole element of the magic pattern with respect to x. Each mapping is represented by five random realizations of the magic pattern in 10×10 supercells grown on (001) $Si_{0.2}Ge_{0.8}$, and the dipole moment averaged over all transitions within 30 meV of the band-gap energy. Unsurprisingly, the transition disappears completely for $x = 0.5$. However, it remains strong for a reasonable amount of mixing (< 0.1).

In conclusion, we have proposed a hitherto a undiscovered material, ($SiGe_2Si_2Ge_2SiGe_n$) grown on (001) Si_xGe_{1-x} with $x \leq 0.4$, which is both direct in crystal momentum space *and* displays a strongly dipole-allowed transition between the VBM and CBM. We have shown that the nature of this material is preserved even after imposing growth-errors swapping Germanium layers for silicon layers. It was shown explicitly that the magic sequence's conduction band minimum is a hybridization of both $\mathbf{\Delta}$ and Γ states, and that the CBM is localized

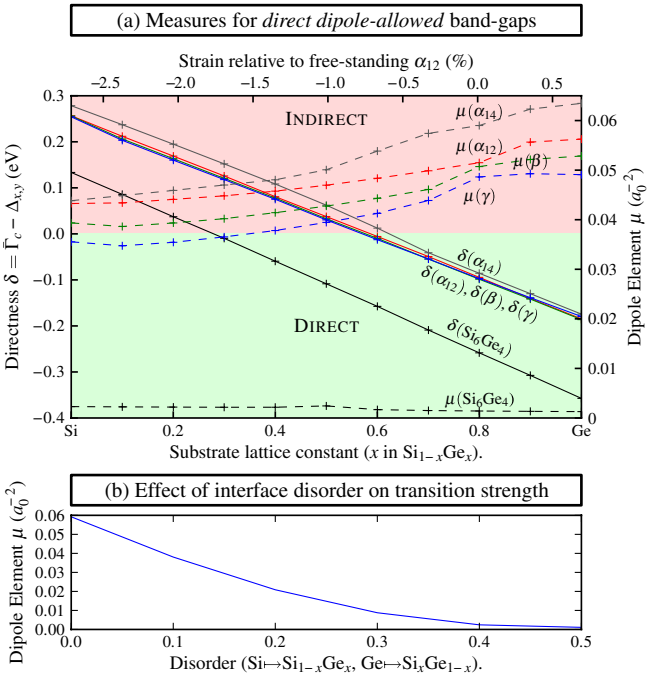

FIG. 3 (color online). (a) A dipole-allowed direct-gap material must present two distinct and necessary properties: (i) CBM and VBM are at the same location in crystal momentum space, and (ii) the transition between CBM and VBM is optically allowed. These two conditions are illustrated here for Si_6Ge_4, α_{12} (magic sequence), α_{14}, β, and γ superlattices, with respect to the substrate $Si_{1-x}Ge_x$. The solid lines measure the energy difference between the conduction band $\vec{\bar{\Gamma}}_c$ and at the in-plane $\vec{\Delta}_c$. It is positive only when (i) is satisfied. The dashed line represent the dipole elements between the VBM and conduction band at $\vec{\bar{\Gamma}}$. The superlattices discovered in this Letter show dipole elements much larger than the previous state-of-the-art Si_6Ge_4. (b) Effect of interface mixing on dipole transitions: interface mixing is modeled by replacing pure Si with $Si_{1-x}Ge_x$ and Ge with Si_xGe_{1-x} within the magic pattern and its edge (defined as two monolayers). For $x = 0$, there is no mixing, and at $x = 0.5$, the pattern has disappeared completely, since there is no contrast between Si rich and Ge rich layers.

mostly over the silicon-rich motif whereas the VBM is delocalized across the motif and the Ge buffer. The particular motif making up the magic sequence was discovered using an intensive inverse band design approach which couples a genetic-algorithm search with a semiempirical electronic structure Hamiltonian. Based on the $SiGe_2Si_2Ge_2SiGe_n$ superlattice discovered in this Letter, it should be possible to design highly efficient CMOS-compatible light emitters and detectors. This will pave the way towards realization of the long sought-after optical-connectors on Si CMOS chips.

This research was supported by the U.S. Department of Energy, Office of Basic Sciences, Division of Materials Sciences and Engineering, Energy Frontier Research Center for Inverse-Band Design, under Grant No. DE-AC36-08GO28308 to NREL.

[1] W. Ng, M. A. Lourenco, R. M. Gwilliam, S. Ledain, G. Shao, and K. P. Homewood, Nature (London) **410**, 192 (2001).
[2] M. du Plessis, H. Aharoni, and L. Snyman, IEEE J. Sel. Top. Quantum Electron. **8**, 1412 (2002).
[3] B. Zheng, J. Michel, F. Y. G. Ren, L. C. Kimerling, D. C. Jacobson, and J. M. Poate, Appl. Phys. Lett. **64**, 2842 (1994).
[4] F. Zhang, V. H. Crespi, and P. Zhang, Phys. Rev. Lett. **102**, 156401 (2009).
[5] D. X. Li and J. Y. Feng, Appl. Phys. Lett. **92**, 243117 (2008).
[6] D. Li, L. Lin, and J. Feng, Physica (Amsterdam) **42E**, 1583 (2010).
[7] J. Kouvetakis, J. Menendez, and A. Chizmeshya, Annu. Rev. Mater. Res. **36**, 497 (2006).
[8] S. Froyen, D. M. Wood, and A. Zunger, Phys. Rev. B **36**, 4547 (1987).
[9] T. P. Pearsall, J. M. Vandenberg, R. Hull, and J. M. Bonar, Phys. Rev. Lett. **63**, 2104 (1989).
[10] M. Ikeda, K. Terakura, and T. Oguchi, Phys. Rev. B **45**, 1496 (1992).
[11] N. Barricelli, Methodos 45 (1954).
[12] A. Franceschetti and A. Zunger, Nature (London) **402**, 60 (1999).
[13] M. A. Green, J. Zhao, A. Wang, P. J. Reece, and M. Gal, Nature (London) **412**, 805 (2001).
[14] L. Tsybeskov, D. J. Lockwood, and M. Ichikawa, Proc. IEEE **97**, 1161 (2009).
[15] A. F. Starace, Phys. Rev. A **3**, 1242 (1971).
[16] L. W. Wang and A. Zunger, Phys. Rev. B **51**, 17 398 (1995).
[17] J. E. Bernard and A. Zunger, Phys. Rev. B **44**, 1663 (1991).
[18] R. Zachai, K. Eberl, G. Abstreiter, E. Kasper, and H. Kibbel, Phys. Rev. Lett. **64**, 1055 (1990).
[19] K. A. Johnson and N. W. Ashcroft, Phys. Rev. B **54**, 14 480 (1996).
[20] L. W. Wang, L. Bellaiche, S. H. Wei, and A. Zunger, Phys. Rev. Lett. **80**, 4725 (1998).